Yeganeh, Maryam; Cheng, Qiang; Dharamsi, Aishwarya; Karimkashi Arani, Shervin; Kuusela-Opas, Juho; Kaario, Ossi; Larmi, Martti

Visualization and comparison of methane and hydrogen jet dynamics using schlieren imaging

Published in:
Fuel

DOI:
10.1016/j.fuel.2022.125762

Published: 01/01/2023

Document Version
Publisher's PDF, also known as Version of record

Fuel 331 (2023) 125762

Contents lists available at ScienceDirect

Fuel

journal homepage: www.elsevier.com/locate/fuel

Full Length Article

Visualization and comparison of methane and hydrogen jet dynamics using schlieren imaging

Maryam Yeganeh *, Qiang Cheng, Aishwarya Dharamsi, Shervin Karimkashi, Juho Kuusela-Opas, Ossi Kaario, Martti Larmi

Department of Mechanical Engineering, Aalto University, School of Engineering, 02150 Espoo, Finland

ARTICLE INFO

Keywords:
H_2 and CH_4 jet
Schlieren imaging
Pressure ratio
Needle lift
Hollow-cone nozzle
Single-hole nozzle

ABSTRACT

In the present work, methane (CH_4) and hydrogen (H_2) jet dynamics from a hollow-cone piezoelectric injector are experimentally investigated. The jet characteristics are studied under the effect of (1) pressure ratio, which is the ratio of the injection pressure (P_i) to the chamber pressure (P_{ch}), (2) needle lift, and (3) nozzle geometry (hollow-cone outwardly opening nozzle without any caps versus the same nozzle with a single-hole cap). Z-type schlieren imaging is applied in a constant volume chamber equipped with optical access. The main characteristics of CH_4 and H_2 jets, i.e., penetration and cross-sectional area, are compared via MATLAB-based image post-processing. The novelty originates from the comparison of H_2 and CH_4 jet characteristics in similar conditions, from two different nozzle geometries, and investigating the effect of pressure ratio by changing the injection pressure and chamber pressure, separately. The results show that a 20% increase in the pressure ratio leads to at least a 13% increase in the H_2 jet penetration and a 20% increase in its cross-sectional area. For CH_4, the same rise in the pressure ratio enhances the jet penetration by at least 17% and its cross-sectional area by at least 21%. Change of P_i or P_{ch} at the same pressure ratio leads to at least 3% and 10% difference in H_2 and CH_4 jet penetration, respectively, and at least 4% difference in their cross-sectional area. Increasing the needle lift leads to a greater jet penetration and cross-sectional area because of a larger injected mass and thereby a larger jet momentum, as well. Moreover, placing a single-hole cap on the hollow-cone outwardly opening nozzle causes approximately 50% pressure loss. However, the single-hole jet can still provide deeper penetration and enough cross-sectional area for efficient mixing. Overall, the comparison of H_2 and CH_4 jet characteristics shows that despite the large differences between their physical properties, jet penetrations are almost similar whereas the H_2 jet possesses at least a 3.5% larger cross-sectional area than CH_4.

1. Introduction

Global warming and air pollution have raised considerable concerns over the past decades since about 80% of energy production is originating from fossil fuels [1]. One viable option for the transition to zero-carbon emissions is to utilize alternative carbon–neutral or low-emission fuels in internal combustion engines, which are one of the major sources of air pollution in the transport sector [2].

In internal combustion engines, the idea of applying H_2 or CH_4 as an alternative fuel seems promising because of numerous advantages. H_2 is a carbon-free energy carrier that can moderately affect greenhouse gas emissions of internal combustion engines since it can utilize readily available manufacturing and distribution infrastructures [3]. Moreover, clean H_2 production by means of biomass and solar-based methods [4,5] is replacing the current state of the art, which is mainly based on natural gas steam reforming [6] and coal partial oxidation [7]. Meanwhile, CH_4 is the main component of natural gas (~95%), which is the cleanest fossil fuel available in many reservoirs in the world [8]. In addition, CH_4 has not only a high H/C ratio, which can reduce CO_2 emission during combustion, but it also has the potential to achieve carbon neutrality from biomass or Sabatier reaction using H_2 and CO_2[9].

Currently, for fuel injection, many automotive manufacturers apply port fuel injection [10,9]. However, a problem with the port fuel injection is low volumetric efficiency and fuel short-circuit from the inlet to the exhaust, which results in lower peak torque and output power [8,10,9]. Direct injection can resolve this problem by injecting the fuel during and/or after the inlet valve closure [10,9]. Furthermore, the direct injection concept can eliminate the possibility of backfire [11]

* Corresponding author.
E-mail address: maryam.yeganeh@aalto.fi (M. Yeganeh).

https://doi.org/10.1016/j.fuel.2022.125762
Received 4 May 2022; Received in revised form 12 July 2022; Accepted 20 August 2022
Available online 2 September 2022

and knocking [12] of the port fuel injection hydrogen engines [10] and lead to higher thermal efficiency as well as lower engine emissions and fuel consumption in natural gas engines [8,13,14,15,16].

The most important aspect of a direct injection gaseous fuel engine is fuel/air mixing efficiency because it can highly affect the combustion quality and engine emissions. Mixing efficiency defines how well the fuel is mixed with the air and how much the fuel/air mixture is homogenous or stratified. As mixing efficiency mainly relies on the gas jet characteristics i.e., the jet cross-sectional area [10], the first goal of combustion and emissions optimization studies is to investigate the gas jet characteristics. It should be also noted that the mixture preparation of the gaseous fuels is typically slower than that of the liquid fuels due to the lower tendency of the gaseous fuels for transferring momentum to the surrounding air [17]. In other words, since gas jets possess lower density and momentum compared to liquid sprays, providing the required amount of the gaseous fuel into the cylinder is challenging [16]. Hence, considering the above-mentioned points, investigating the gas jet behavior is of paramount importance in developing direct injection gaseous fuel engines which is one of the main purposes of the current study.

In the context of CH_4 or natural gas, extensive efforts have been devoted to discovering the parameters affecting fuel/air mixing. For instance, Yu et al. [18,19,20] investigated the effect of pressure ratio on the natural gas jet behavior and reported that increasing the pressure ratio even up to the limit of reaching the transient or highly under-expanded jet, can increase the mixing efficiency. They also studied the flow structure and mixture formation of low-pressure ratio wall-impinging jets and showed that placing a wall as an obstacle against the jet penetration can improve the mixing [21,22]. Kuensch et al. [16] investigated the natural gas jet behavior injected by a hollow-cone piezoelectric injector, as well. They noted that increasing the injection pressure and the needle lift results in a better hollow-cone jet expansion, which may eventually lead to better mixing. Additionally, Sankesh et al. [9] studied the natural gas jet characteristics from an outwardly opening nozzle for the direct injection engines and found that mixing improves with time because jet concentration decreases with time evolution. Moreover, Vera-Tudela et al. [23] investigated the effect of needle dynamics on the penetration of a high-pressure methane jet. They realized that the needle dynamics strongly depend on the injection pressure and the chamber pressure rather than the pressure ratio. Furthermore, they showed that compared to the injection pressure effect on the jet penetration, the chamber pressure effect is of more significance.

For H_2, there are a few studies on the parameters affecting its mixing characteristics. Applying port fuel injection and spark ignition technologies for H_2 has gained attention [10,24,25,26,27,28]; however, the idea behind the H_2 direct injection compression ignition engine is quite recent [29]. In this respect, several studies have contributed to the investigation of the jet or combustion behavior of H_2 or H_2-CH_4 blends. For example, Abdul Rahman et al.[30] investigated the local concentration of hydrogen transient jets and found that increasing the ambient pressure can decelerate the jet penetration. Likewise, Deng et al. [31] characterized the hydrogen jet behavior in an argon environment and showed that by increasing the injection time, the injection pressure and the ambient pressure could result in a deeper jet penetration. Takagi et al. [32] also suggested applying the plume ignition combustion concept (PCC) in a direct injection hydrogen engine to optimize the injection timing, jet plume location, and jet geometry which resulted in a higher thermal efficiency and near-zero emissions. Furthermore, Wang et al. [33] studied the combustion characteristics of H_2-natural gas and showed that turbulence intensity highly affects the turbulent combustion of the gaseous fuel.

With relevance to the presented literature review, there are two evident research gaps that can be addressed in the present work: 1) a better insight into the parameters affecting the H_2 and CH_4 jet characteristics (e.g., pressure ratio, injection pressure, chamber pressure, needle lift, and nozzle geometry), and 2) a comparison of the H_2 and CH_4 jet characteristics under similar conditions for the future design and optimization of the direct injection compression ignition gaseous fuel engines. In this regard, the main objectives of this work are to:

1) measure the H_2 and CH_4 jet penetration and cross-sectional area.
2) assess the effect of the pressure ratio on the H_2 and CH_4 jet characteristics by changing the injection pressure and chamber pressure, separately.
3) assess the effect of the needle lift on the H_2 and CH_4 jet dynamics.
4) assess the effect of nozzle geometry (a hollow-cone outwardly opening nozzle without any caps versus the same nozzle with a single-hole cap) on the H_2 and CH_4 jet behavior.
5) simultaneously analyze and compare the H_2 and CH_4 jet development in similar conditions.

The novelty mainly originates from objectives 2, 4, and 5. The outline of this paper is as follows. Section 2 explains the experimental set-up and methodology. Section 3 systematically analyzes the effect of variables, i.e., pressure ratio and needle lift on the H_2 and CH_4 jet dynamics and characteristics. In addition, the effect of two different nozzle geometries (a hollow-cone outwardly opening nozzle without any caps versus the same nozzle with a single-hole cap) on the jet behavior is discussed. Lastly, the conclusions are presented in Section 4.

2. Experimental setup and methodology

In this section, the experimental setup and its components, the optical system, the test matrix, the image post-processing method, and the error analysis are described, respectively.

2.1. Experimental setup

The experimental setup consists of four major circuits: 1) injection line, 2) chamber pressurizing line, 3) exhaust line, and 4) control system. First, the gas injection line is a 3-meter hose from the H_2 or CH_4 bottle to the injector on which a pressure regulator and a pressure sensor are installed for adjusting and monitoring the injection pressure. It should be mentioned that the length of the hose (3 m) seems to be enough to keep the injection pressure constant during the injection phase based on numerical simulations by GT-power [34]. Second, the chamber pressurizing line from the nitrogen bottle rack to the constant volume chamber consists of a pressure regulator, a hose, and a needle valve right before the chamber. Third, the exhaust line possesses 1) a spring relief valve for releasing the pressure when reaching the maximum chamber pressure, 2) a shut-off valve to empty the chamber, and 3) a regulating spring valve to regulate the chamber pressure with the gas supply. Finally, the LabVIEW software [35] and a driver from National Instrument [35] are employed for the injector and the high-speed camera (Phantom V2012) synchronization. The software is connected to a pressure and a temperature sensor to monitor the chamber pressure and temperature, as well.

Fig. 1 shows the test setup and the hollow-cone outwardly opening injector which is a commercial injector for gasoline direct injection for rail pressures up to 200 bar from Siemens VDO Automotive. As it is shown in the cross-section view of the injector, the needle is directly activated by a piezoelectric stack driven by the control unit from National Instruments to set the voltage level and the current profile for controlling the needle lift opening and closing speed.

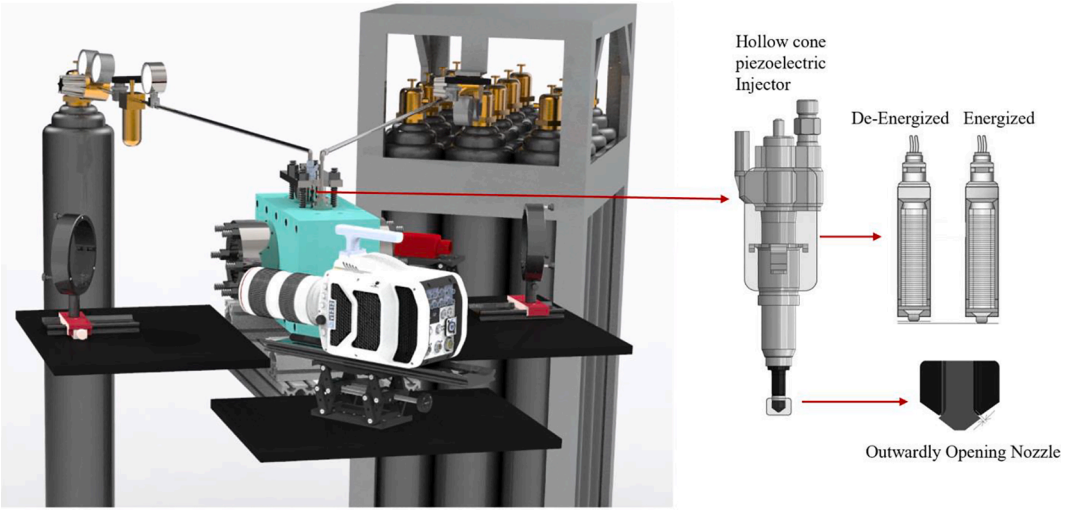

Fig. 1. Schematic of the test setup and injector.

2.2. Optical measurements

In this study, high-speed z-type schlieren imaging is applied for visualizing the gas jet. In fact, the schlieren system is a shadowgraph with a schliere (knife or razor blade(iris)) and works such that the light rays are bent whenever they see changes in the density of a fluid. In the z-type schlieren system, lenses are replaced by parabolic concave mirrors because of two advantages. First, unlike lenses, mirrors do not suffer from chromatic aberrations. Second, achromatic lenses, which must be utilized to minimize the chromatic aberrations, are expensive especially if a large free diameter is required [36].

Fig. 2 demonstrates a schematic of the high-speed z-type schlieren system. In this system, first, the jet is illuminated by a collimated light beam from a high-power monochromatic LED spotlight and a mirror. Then, the jet refracts the light, and the other mirror concentrates the beam into the lens of the high-speed camera which is located behind an iris. This iris partly blocks the refracted light beams to generate the schlieren image. Furthermore, because of the high chamber pressures and the safety issues related to that, the injector should be mounted on top of the chamber and the visualization should be through the quartz lateral windows. Including windows in the optical path of the schlieren system might reduce the image quality [36] but this problem is solved by means of background subtraction in image post-processing. Table 1 provides a detailed list of the components of the optical system.

Table 1
Optical system components.

Component	Feature
Electrical power of the LED	21 W (30% of the Maximum Power of 70 W)
Diameter of aperture's slit	3 mm
Focal length of first mirror	609,6 mm
Focal length of second mirror	762 mm
Percentage of the knife-edge cut-off	Approximately 60%
Exposure time of the camera	10 μs
Frame rate	34,000
Resolution	768 × 768

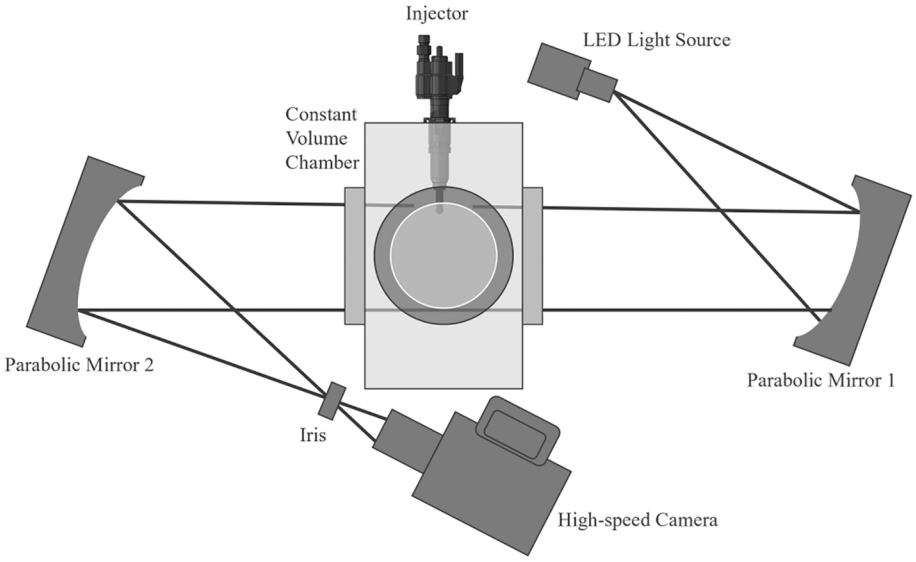

Fig. 2. Schematic of the z-type schlieren imaging system.

2.3. Experimental matrices

Jet penetration and cross-sectional area are the two main global jet characteristics that are measured at 16 test points at the standard room pressure (1 atm) and temperature (25 °C). The experimental test matrix for investigating the effect of the pressure ratio (pr = P_i/P_{ch}) and the needle lift on the jet behavior are represented in Table 2. It should be also mentioned that there are 10 repetitions for each test and the injection duration for all the measurements is 5 ms which is shown by the red dashed line on the plots of jet characteristics in the results section.

Table 2
Experimental matrix.

Variable	pr	P_i(bar)	P_{ch}(bar)	Needle Lift (μm)
(1) Effect of pressure ratio by changing P_i at constant P_{ch}	8, 12, 16 and 20	40, 60, 80 and 100	5	25
	4, 6, 8 and 10	40, 60, 80 and 100	10	25
	2, 3, 4 and 5	40, 60, 80 and 100	20	25
(2) Effect of pressure ratio by changing P_{ch} at constant P_i	8, 4 and 2	40	5, 10 and 20	25
	12, 6 and 3	60	5, 10 and 20	25
	16, 8, and 4	80	5, 10 and 20	25
	20, 10 and 5	100	5, 10 and 20	25
(3) Effect of needle lift	10	100	10	20, 25, 30, 35, and 40

2.4. Image post-processing

A MATLAB code is developed for image post-processing. Fig. 3 indicates the steps of image post-processing. As it can be seen, first, the code subtracts the background from the image by means of an average of the first images which were taken before the start of injection. Then, the code starts filling the holes of the jet because it expects that there are no holes inside the jet. After that, the code removes the shadows and the small objects from the image. Finally, the code traces the boundaries of the jet in accordance with the selected threshold value for all repetitions and it presents the mean value of the jet penetration and cross-sectional area as the results. The jet penetration is defined as the distance along the jet axis to the boundary of the jet and the jet cross-sectional area is the area within the jet boundaries as shown in Fig. 3, step 9. The injector tip diameter is also measured physically to calibrate all the images and avoid errors in calculating the jet characteristics (penetration and cross-sectional area).

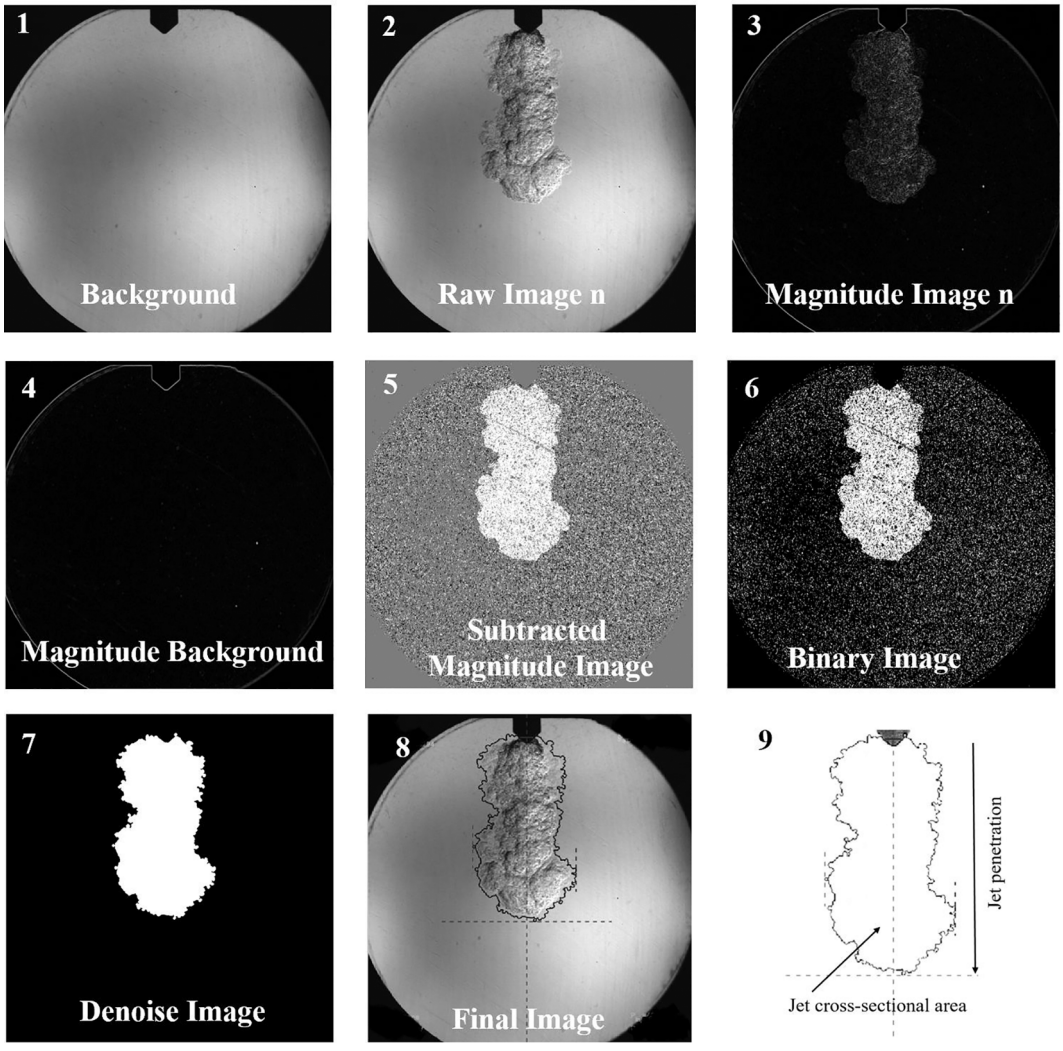

Fig. 3. Image post-processing steps.

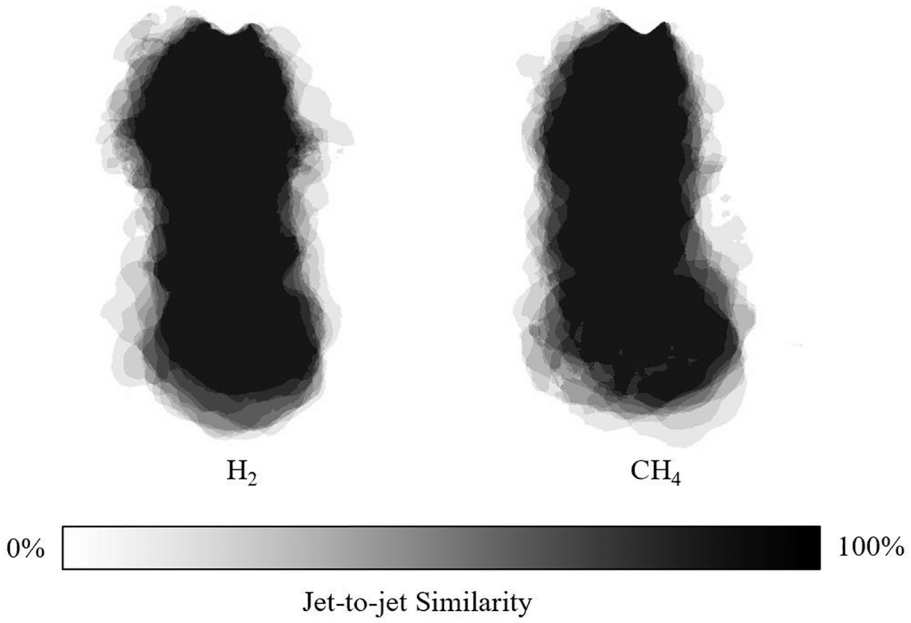

Fig. 4. Jet behavior in different repetitions.

2.5. Error analysis

There were 3 main origins for error in the jet parameters. First, the jet-to-jet variation error which was addressed by repeating each experiment 10 times. To ensure the similarity of the jet behavior between the repetitions of each experiment, a custom Python code is developed. Fig. 4 indicates the promising consistency of the jet behavior in different repetitions for both H_2 and CH_4 which assures that the number of repetitions is enough. The difference between the minimum and maximum jet-to-jet variation is also shown via error bars on the jet characteristics plots in the results section. However, to avoid poor images with too many details, the error bars are selected at every 15 frames. Second, the error in the injection and chamber pressure gauges which are with ±0.5% of full-scale output accuracy. Third, the image post-processing error in which the jet penetration and cross-sectional area calculations cover up to 95% of the maximum horizontal penetration of the jet.

3. Results and discussions

This section provides the results of the experimental campaign. First, a comparison between the CH_4 and H_2 jet structures is described. Then, the effect of the pressure ratio and the needle lift on the H_2 and CH_4 jet penetration and cross-sectional area are compared. Finally, the current results and the results of a previous study on the same jets from the same injector nozzle but with a single-hole cap on the nozzle exit, are compared at one test point to analyze the differences between the jet characteristics from two different nozzle geometries.

3.1. Jet structure

As the main purpose of this study is to compare the behavior of H_2 and CH_4 gas jets, it is essential to first observe the jet structure through consecutive time intervals. Fig. 5 shows the comparison of CH_4 and H_2 jet structure at pr = 10 (P_i = 100 bar/ P_{ch}=10 bar), and needle lift = 25 μm within consecutive time intervals of 0.8823 ms.

Fig. 5 shows that compared to CH_4, the H_2 jet is not only wider but has also a shorter penetration length. This phenomenon can be explained by the distinct densities of these gases because H_2 molecule is a light species that can easily diffuse to the surrounding both axially and radially. Graham's law of diffusion also confirms this observation, as it states that "the rate of diffusion or effusion of a gas is inversely proportional to the square root of its molecular weight" [37]. In the same conditions of temperature and pressure, since the molar mass is proportional to the mass density, the rate of diffusion of a gas (r) is inversely proportional to the square root of its mass density (d) as it is shown in (Eq.1). In addition, the momentum effect is higher in the CH_4 jet due to its greater molecular weight, which results in a deeper penetration rather than diffusion to the surrounding [10,38].

$$r \propto 1/\sqrt{d} \tag{1}$$

Moreover, while the CH_4 jet has a spherical vortex structure in both the near-field and far-field of the nozzle, the H_2 jet has different morphologies in the near-field and far-field of the nozzle. Consistent with the observations in Fig. 5 and according to Wang et al. [10], H_2 jet has a conical structure in the near-field and spherical in the far-field of the nozzle. It should be also mentioned that H_2 images are darker than CH_4 images because the schlieren imaging is based on density differences and the density difference between H_2 and the surrounding gas is greater than that of CH_4.

3.2. Effect of the pressure ratio

One of the most substantial parameters which can highly affect the jet characteristics is pressure ratio which is the ratio of the injection pressure to the chamber pressure (pr = P_i/ P_{ch}). Pressure ratio defines how fast the fuel expands into the chamber and sets the limit between the subsonic and supersonic flow. If the pressure ratio exceeds the minimum pressure ratio for the choked condition [39], the flow will be supersonic or highly under-expanded which is the case for all the measurements in the current study. At choked flow conditions, the pressure ratio is the most dominant parameter affecting the mass flow [20]. In addition, higher pressure ratios can lead to higher turbulence levels and faster mixing [40] which are particularly influential for direct injection engines. In this study, the effect of pressure ratio on the jet characteristics both by changing P_i at a constant P_{ch} and by changing P_{ch} at a constant P_i is investigated. This is because injection pressure and chamber pressure might affect the jet behavior differently [23]. Fig. 6 shows the effect of increasing the pressure ratio by increasing P_i (from

60 to 100 bar at constantP_{ch} = 20 bar) on the jet structure. As it can be seen, an increase in P_i can enhance both H_2 and CH_4 jet penetration and diffusion to the surrounding which results in efficient mixing. However, H_2 seems to have a better mixture formation because it possesses a larger cross-sectional area than CH_4.

The effect of pressure ratio on the jet behavior by changing P_{ch} (from 10 to 20 bar) at constantP_i = 100 bar is also demonstrated in Fig. 7. As it is shown, increasing P_{ch} leads to an increase in the drag force against the jet expansion which results in a larger jet spread angle (cross-sectional area) and a reduced jet penetration for both H_2 and CH_4. Hence, the preliminary view of the jet structure displays that chamber pressure can significantly affect the mixture formation.

Fig. 8 (a)-(c) shows the effect of pressure ratio by changing the injection pressure at a constant chamber pressure on the jet penetration and cross-sectional area with time evolution. According to the plots of the jet penetration versus time, rising the P_i leads to deeper penetration of both H_2 and CH_4 jets which is consistent with the results of several studies i.e., [15,16,17,18,19,20,21,22]. The main reason is that higher injection pressure means a higher pressure ratio and accordingly a higher mass flow. Since for both H_2 and CH_4, the flow is choked, the mass flow tends to vary with the pressure ratio. In contrast, increasing the chamber pressure results in the suppression of this trend because of a lower pressure difference between the ambient and the injected jet [23 41] and the increased drag force against the jet expansion [42]. Furthermore, while at lower injection pressures (40 and 60 bar) CH_4 shows a deeper jet penetration, at higher injection pressures (80 and 100 bar), H_2 depicts a deeper jet penetration. As previously stated, the reason is that at lower injection pressures, H_2 easily diffuses in all directions whereas CH_4 mostly diffuses axially because of the momentum effect due to its greater molecular weight [10,37,38]. It should be also mentioned that although the higher injection pressures lead to a higher jet momentum, the wider jet cone angle can cause a stronger aerodynamic drag that limits both the jet penetration and tip velocity [15]. The other noticeable point is that although H_2 and CH_4 physical properties are not similar, the trend of their penetration is extremely close to each other, especially during the injection time. That is because the jet

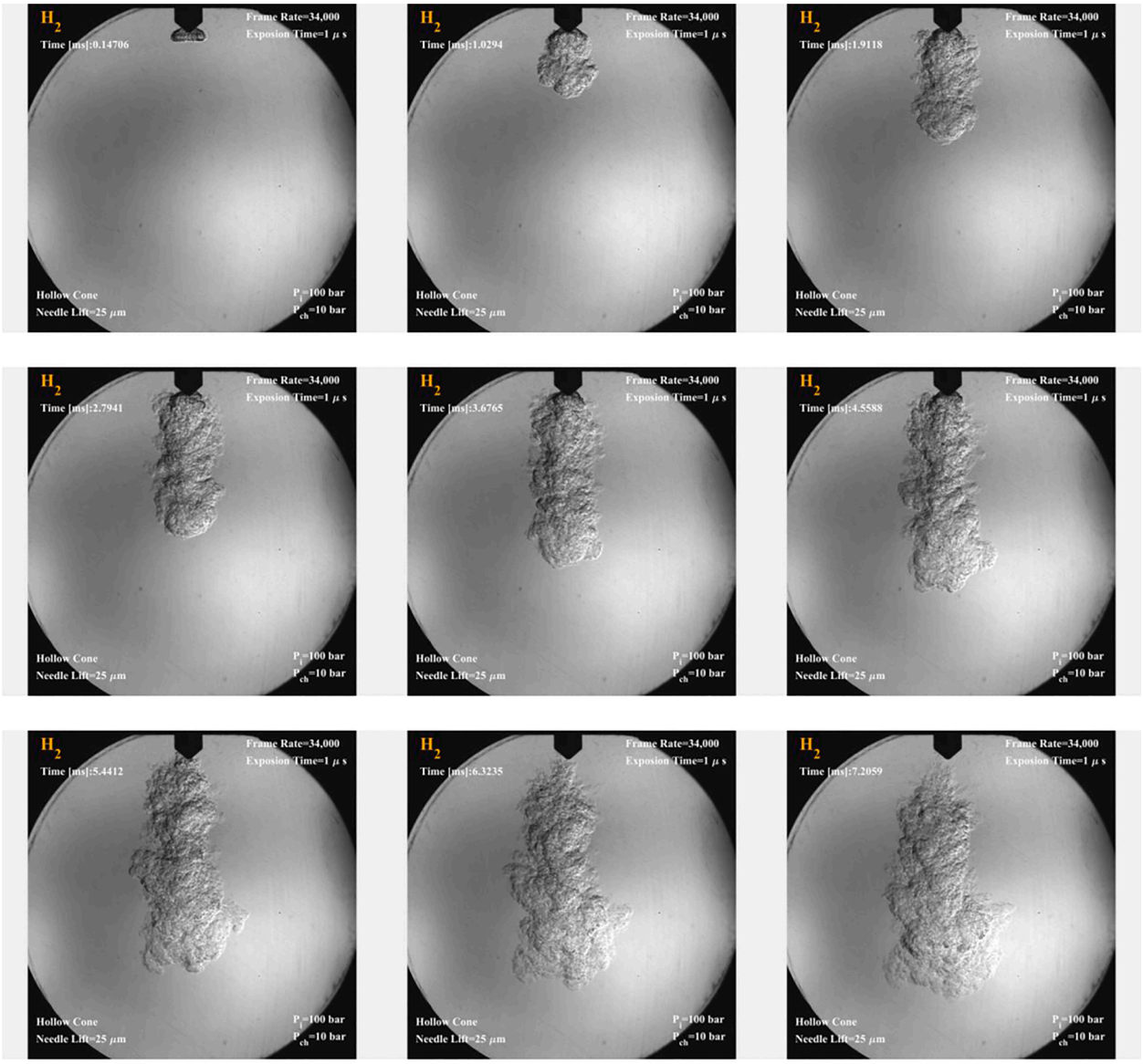

(a) H_2 jet evolution

Fig. 5. H_2 jet evolution (a) versus CH_4 jet evolution (b).

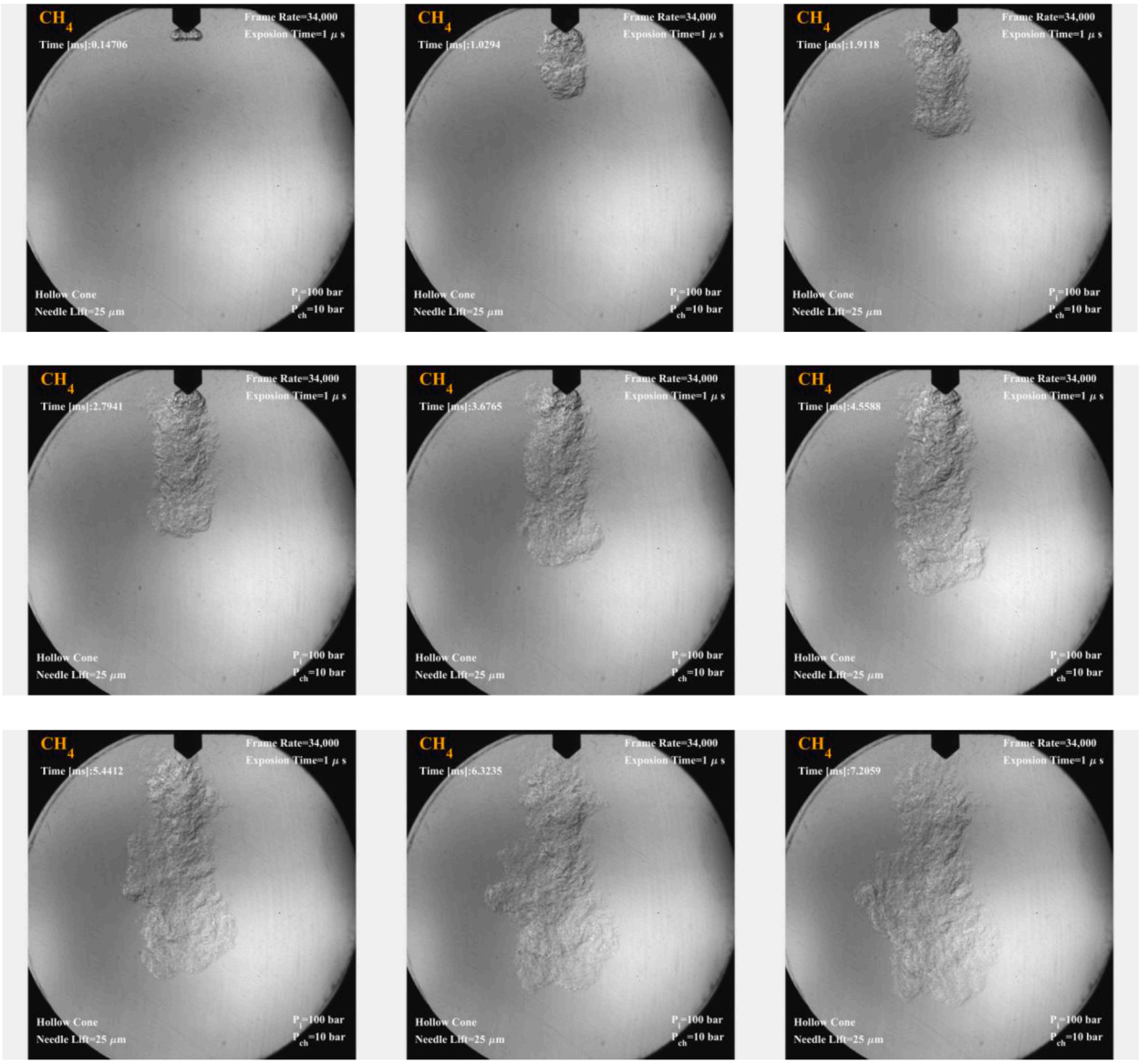

(b) CH_4 jet evolution

Fig. 5. (*continued*).

development phase is mostly affected by the initial momentum [15] and gases start to follow their intrinsic diffusion after the end of injection (valve closure). Even after the end of injection, the maximum difference between H_2 and CH_4 penetration remains only 11% atP_i = 80 bar andP_{ch} = 10 bar.

Furthermore, in Fig. 8, plots of the jet cross-sectional area versus time indicate that apart from the type of the injected gas, higher injection pressures result in larger jet cross-sectional areas. In other words, higher injection pressures provide a wider spatial distribution of the injected gas in the surrounding, which is the main representative of mixing efficiency [16]. In addition, as expected, the cross-sectional area of the H_2 jet is larger than that of CH_4 in all cases which confirms that H_2 can provide a better mixture formation, especially at lower injection and chamber pressures. Fig. 8 also shows that the largest gap between the cross-sectional areas of the H_2 and CH_4 jets (~21.5%) is related to the lowest injection and chamber pressure. Additionally, raising the chamber pressure does not only restrict the jet spatial distribution but also linearizes the growth trend of the jet cross-sectional area.

Table 3 shows the maximum differences between the CH_4 and H_2 jet characteristics at each pressure ratio.

Fig. 9 (a)-(d) depicts the effect of pressure ratio by changing the chamber pressure at a constant injection pressure on the jet characteristics with time progress. According to the plots of the jet penetration versus time, increasing the chamber pressure suppresses both H_2 and CH_4 jet penetration; however, the trend of their penetration varies quite similarly. This might be explained by a justification in [42] on diesel spray which states that raising the chamber pressure increases the drag and decelerates fuel droplets because of a higher probability of

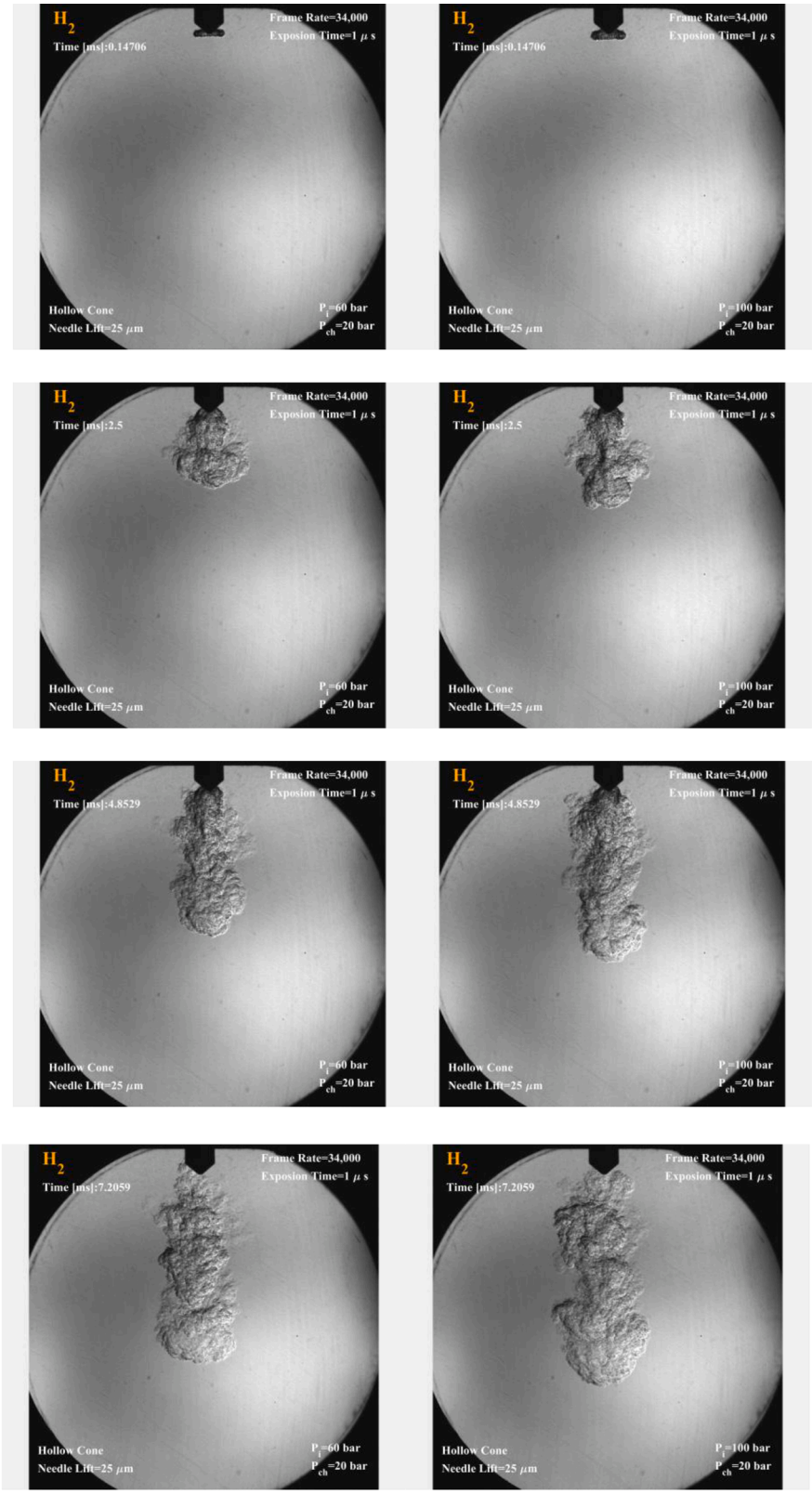

(a) Effect of pressure ratio by increasing P_i from 60 bar (left) to 100 bar (right) on H_2 jet structure

Fig. 6. Effect of pressure ratio on the jet structure by changing P_i at constant P_{ch}.

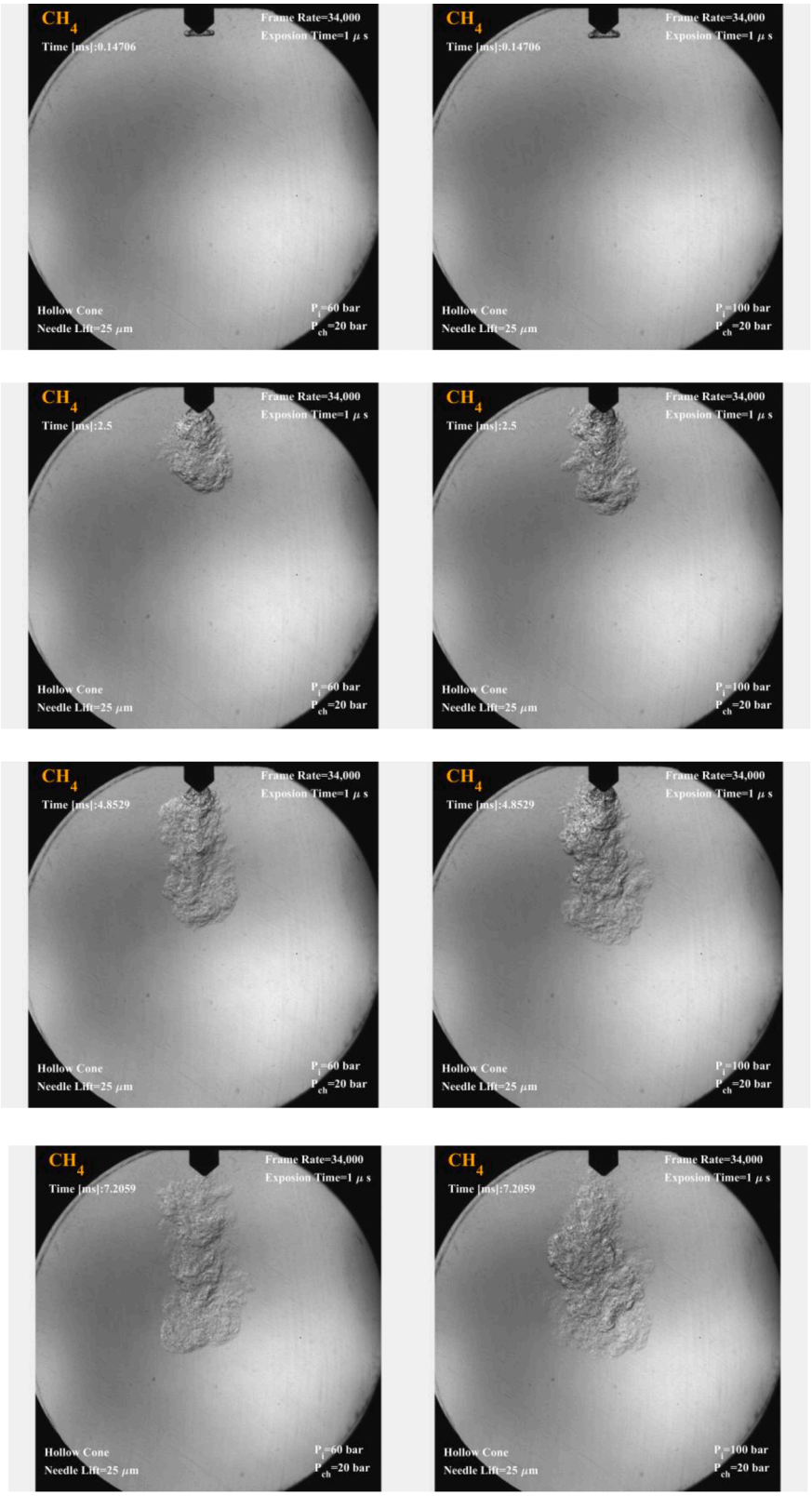

(b) Effect of pressure ratio by increasing P_i from 60 bar (left) to 100 bar (right) on CH_4 jet structure

Fig. 6. (*continued*).

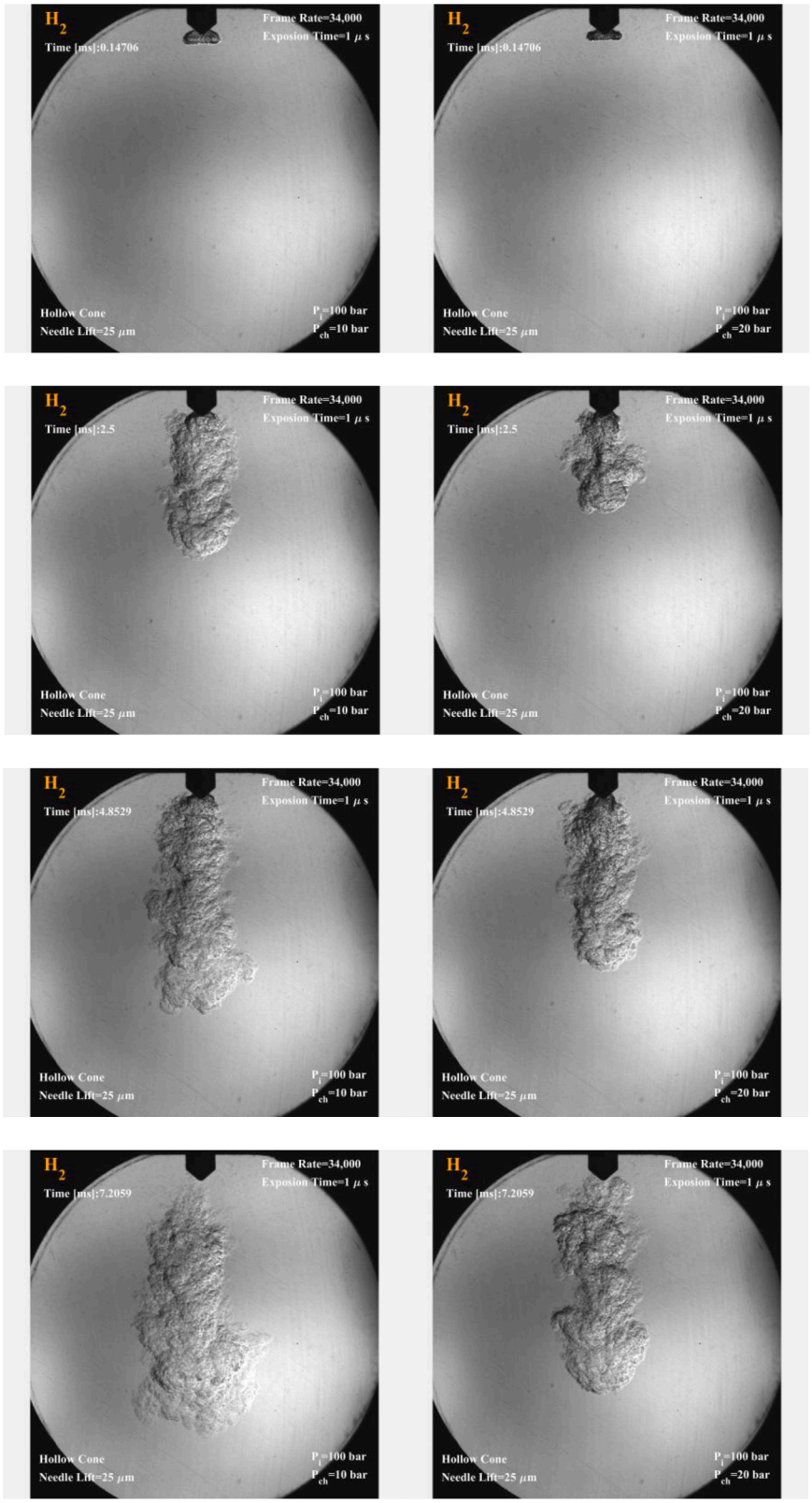

(a) Effect of pressure ratio by increasing P_{ch} from 10 bar (left) to 20 bar (right) on H_2 jet structure

Fig. 7. Effect of pressure ratio on the jet structure by changing P_{ch} at constant P_i.

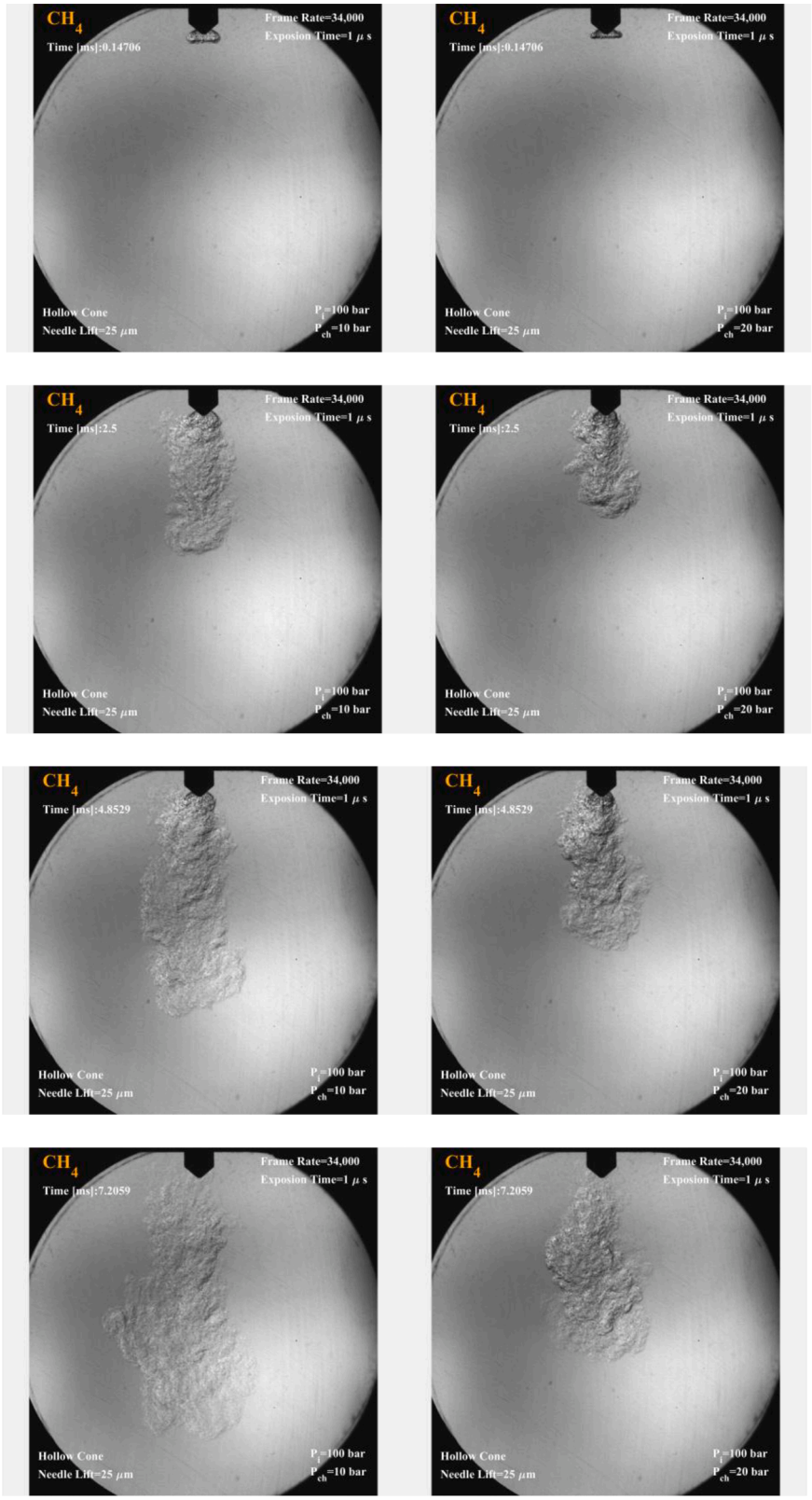

(b) Effect of pressure ratio by increasing P_{ch} from 10 bar (left) to 20 bar (right) on CH_4 jet structure

Fig. 7. (*continued*).

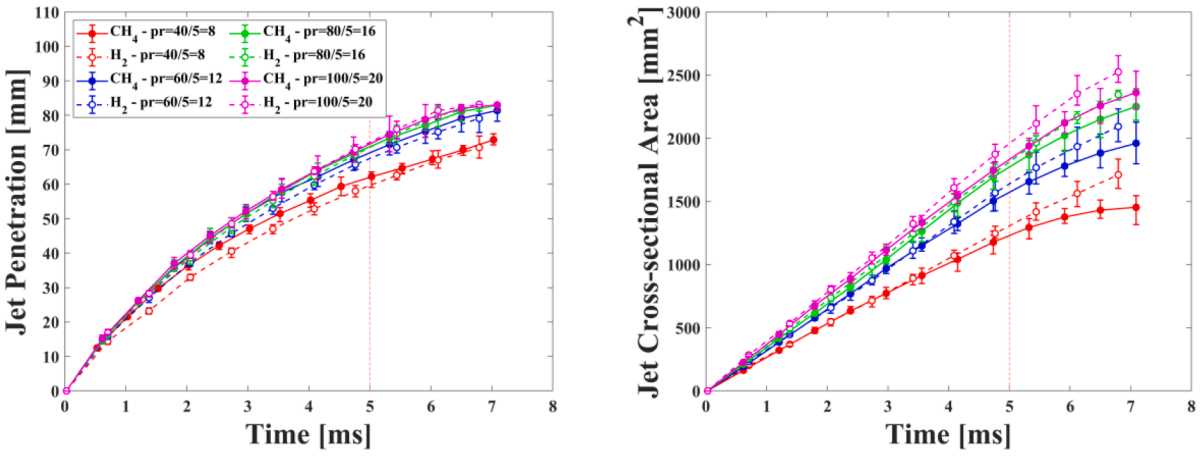

(a) Jet penetration (left) and cross-sectional area (right) at pr =8, 12, 16, and, 20

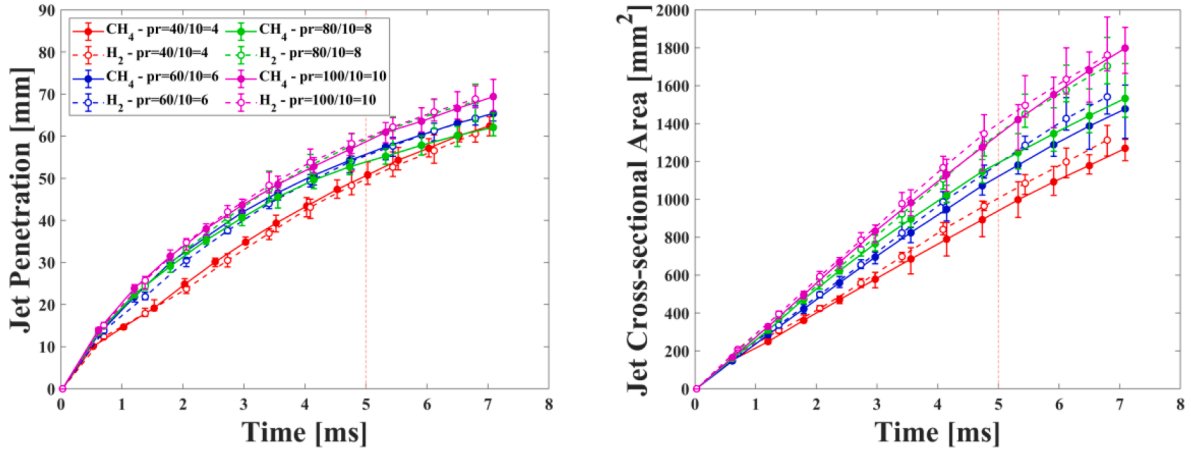

(b) Jet penetration (left) and cross-sectional area (right) at pr =4, 6, 8, and, 10

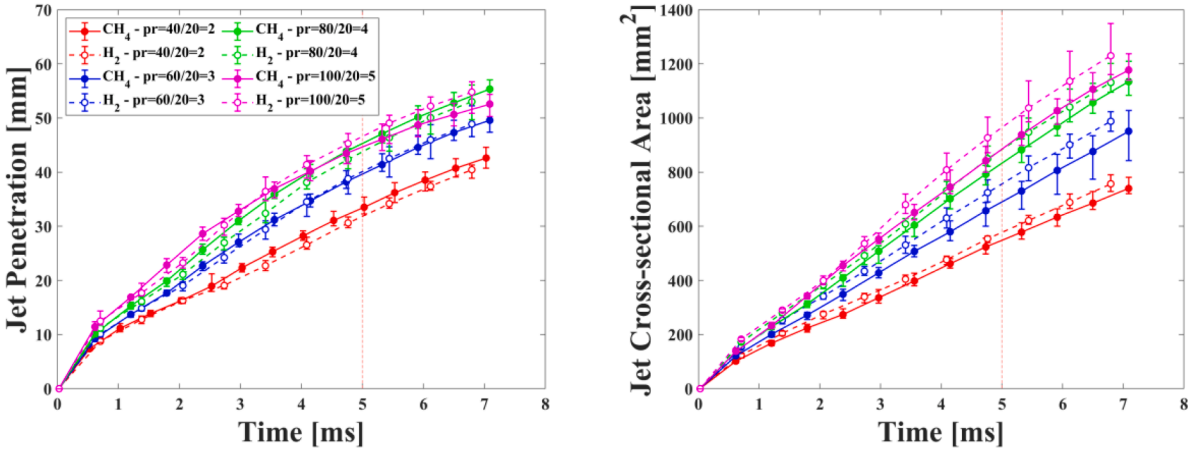

(c) Jet penetration (left) and cross-sectional area (right) at pr =2, 3, 4, and, 5

Fig. 8. Effect of pressure ratio (pr) on the jet characteristics by changing P_i at constant P_{ch}.

coalescence. Although here, a gaseous fuel jet is studied rather than a liquid spray, the same scenario can be employed because increasing the chamber pressure can enhance the drag force against the jet expansion which can decelerate jet particles and keep them nearby each other. In addition, Banholzer et al [41] also showed that the jet penetration is faster at lower chamber pressures due to the smaller densities. Thus, based on these interpretations, the potential for deep penetration can be restricted markedly.

Fig. 9 also illustrates the effect of chamber pressure on the jet cross-sectional area. In accordance with this figure, increasing the chamber pressure results in a reduced jet cross-sectional area for both H_2 and CH_4. Indeed, rising the chamber pressure can either increase the densities [41] or intensify the drag against the jet expansion [42] and linearize the trend of the jet cross-sectional area variation. Furthermore, in all cases, the H_2 jet cross-sectional area is larger than that of CH_4 as a result of the diffusion law, which was discussed earlier. Hence, these results also demonstrate that H_2 tends to produce a better mixture formation.

To quantify the observations on the mixture formation, a new parameter (γ) is defined as the ratio of the injected jet mass (m) to the jet cross-sectional area (A).

$$\gamma = m/A \tag{2}$$

This parameter shows how dense the jet is to provide efficient mixing. γ can be calculated by finding (1) mass flow rate of the flow inside the injector's nozzle and (2) injected mass in the injection duration time.

First, by assuming a control volume around the injector's nozzle, mass flow rate is calculated from:

$$\dot{m} = C_d A_{Nozzle} \sqrt{2\rho\Delta p} \tag{3}$$

where C_d is the nozzle discharge coefficient, A_{Nozzle} is the nozzle cross-sectional area, ρ is the density of the flow inside the nozzle, and Δp is the pressure difference between the flow inside the nozzle (injection pressure) and the ambient (chamber pressure). It is noted that C_d can be assumed 1 for both H_2 and CH_4 jets in the current experiments since the flow is choked and the Reynolds number is high in all test points [43,44,45].

Second, the injected mass can be found by:

$$m = \dot{m}\Delta t \tag{4}$$

where $\dot{m}$ is the mass flow rate form Eq. (3) and Δt is the injection duration time.

As an example, for the conditions presented in Table 4, γ for CH_4 ($36.1 \times 10^{-4} kg/m^2$) is approximately 3 times greater than γ for H_2 ($12.2 \times 10^{-4} kg/m^2$) which means that CH_4 jet is denser, hence, weaker in providing efficient mixing. Since the maximum difference between H_2 and CH_4 jet characteristics is around 10% under the same conditions, it can be concluded that γ of H_2 is always greater than that of CH_4 and consequently, H_2 can always provide a better mixture formation.

Another justification for a better mixing with H_2 is to compare the ratio of the γ to the stoichiometric air/fuel ratio between the H_2 and CH_4 jets because in the direct injection concept, we should notice how much the jet is lean or rich rather than the mixture in the whole chamber. Thus, if we define the ratio of the γ to the stoichiometric air/fuel ratio as ξ in Eq. (5) , for the same mentioned test point in Table 4, the ξ is 21.2×10^{-5} for the CH_4 jet and 3.5×10^{-5} for the H_2 jet. This reveals that the H_2 jet is always leaner than CH_4 jet which can assist the mixing substantially.

$$\xi = \gamma/(A/F)stoic \tag{5}$$

where γ can be calculated from Eq. (2) and (A/F)stoic is the stoichiometric air/fuel ratio which is 34.5 for H_2 and 17 for CH_4.

As a final note to close this section, a comparison of the jet characteristics at the same pressure ratio is displayed in Fig. 10 to strengthen the novelty. As it can be observed, the jet characteristics are not the same at identical pressure ratios. There is at least 3% and 10% difference in the H_2 and CH_4 jet penetration, respectively, and at least 4% difference in their cross-sectional areas. Indeed, the jet penetration and the cross-sectional area are sensitive to the variation of both injection and chamber pressure. However, the jet penetration possesses the largest difference, especially at lower pressure ratios. Hence, similar to the results of [23], it is highly recommended to investigate the effect of the pressure ratio by changing the injection pressure and chamber pressure, separately.

Table 3
Maximum differences between CH_4 and H_2 jet characteristics at different pressure ratios.

pr	P_i	P_{ch}	Penetration Difference (%)	Cross-sectional Area Difference (%)
2	40	20	10	6
3	60	20	4	10
4	80	20	6	7.5
4	40	10	4	9
5	100	20	4	11.5
6	60	10	5.5	4.5
8	40	5	7.5	6.5
8	80	10	9.5	13
10	100	10	4	6
12	60	5	6	4.5
16	80	5	4.5	3
20	100	5	2.5	8

3.3. Effect of the needle lift

Variation of the needle lift of a piezoelectric injector has a great impact on the jet global features i.e., penetration and cross-sectional area [16]. In this study, the change of the needle lift is done by changing the injection charge voltage because they are directly related. Table 5 shows the range of the injection charge voltage, the correspondent needle lift, and the correspondent nozzle cross-sectional area for the applied hollow-cone piezoelectric injector. As it is shown in this table, increasing the injection charge voltage means increasing the needle lift, and increasing the needle lift changes the nozzle cross-sectional area for the fuel flow passing through which contributes to the increase of the mass flow. Hence, changes in needle lift can significantly affect the jet characteristics as well as the mixture formation.

Fig. 11 demonstrates how an increase in the needle lift can change the jet structure. The most remarkable point of this figure is the sharp edge of the jet as a result of raising the needle lift. Since raising the needle lift culminates in injecting a greater mass flow rate along with higher initial momentum, the jet takes on a sharp edge along and deeper axial penetration. Furthermore, since CH_4 has a greater molecular weight and consequently greater intermolecular forces [46], its molecules tend to stay and penetrate much closer to each other. That is why the CH_4 jet has a less sharp edge than the H_2 jet.

Fig. 12 shows the effect of the needle lift on the jet penetration and cross-sectional area at a constant pressure ratio (pr = 10). This figure indicates that apart from the type of the injected gas, increasing the needle lift leads to an increase in the jet penetration and cross-sectional area. Additionally, H_2 jet penetration and cross-sectional area are greater than that of CH_4 for all the cases, especially at minor needle lifts (20 and 30 μm) which is consistent with the diffusion law. Thus, these results also show that not only does the needle lift highly affect jet characteristics and mixing, but also H_2 can provide better mixture formation than CH_4,especially at lower needle lifts. Table 6 shows the maximum differences between CH_4 and H_2 jet characteristics at different needle lifts.

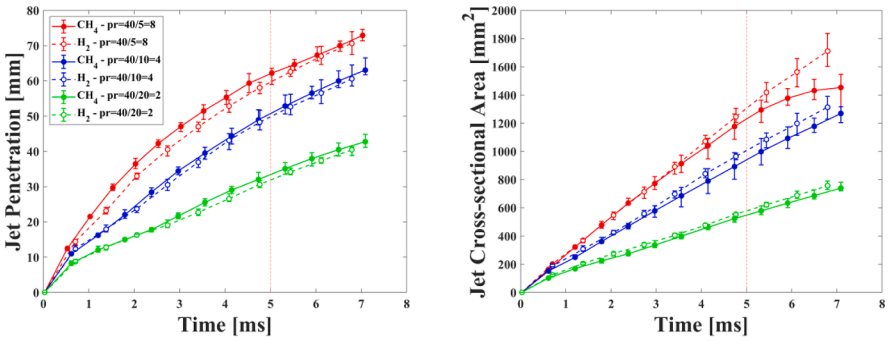

(a) Jet penetration (left) and jet cross-sectional area (right) at pr =2, 4, and, 8

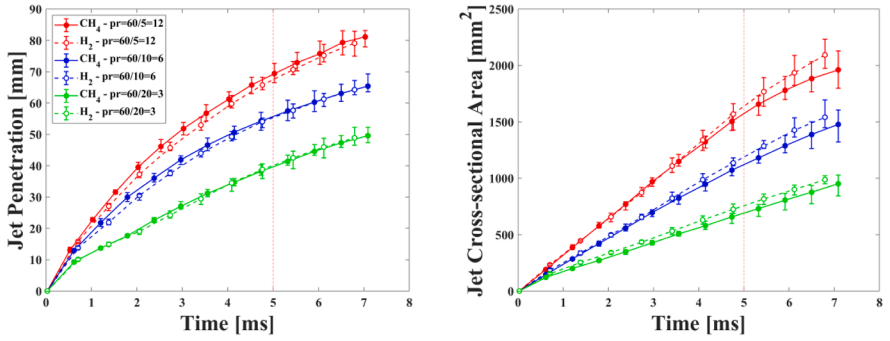

(b) Jet penetration (left) and jet cross-sectional area (right) at pr =3, 6, and, 12

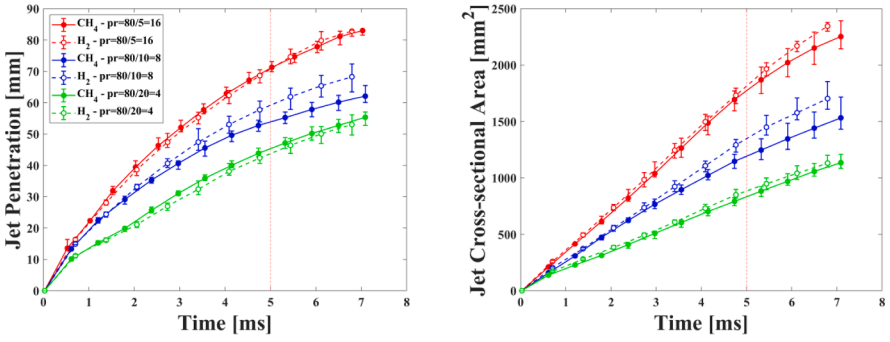

(c) Jet penetration (left) and jet cross-sectional area (right) at pr =4, 8, and, 16

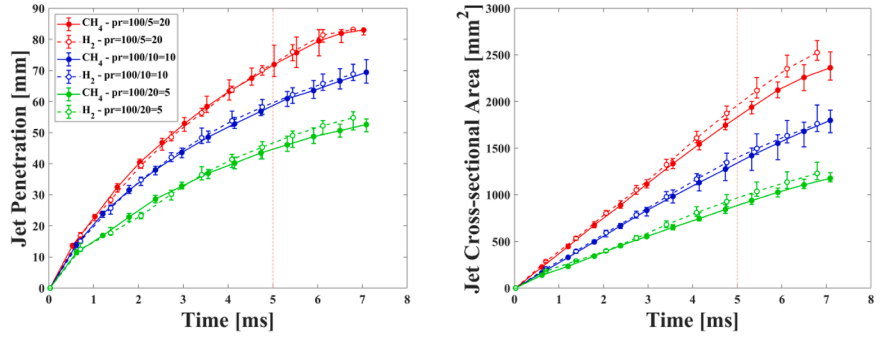

(d) Jet penetration (left) and jet cross-sectional area (right) at pr =5, 10, and, 20

Fig. 9. Effect of pressure ratio (pr) on the jet characteristics by changing P_{ch} at constant P_i.

Table 4
Parameters of one test point as an example for calculating γ.

Parameter	Quantity
Pressure ratio (pr)	20
Injection pressure (P_i)	100 bar
Chamber pressure (P_{ch})	10 bar
Pressure difference (Δp)	90 bar
Injection duration (Δt)	0.005 s
Nozzle cross-sectional area (A_{Nozzle})	$4\times10^{-7} m^2$
H_2 density	0.08375 kg/m^3
H_2 jet cross-sectional area	0.002 m^2
CH_4 density	0.657 kg/m^3
CH_4 jet cross-sectional area	0.0019 m^2

Table 5
Injection charge voltage and the correspondent needle lift and nozzle cross-sectional area.

Injection Charge Voltage (V)	Needle Lift (μm)	Nozzle Cross-sectional Area (mm^2)
90	20	0.35
100	25	0.4
110	30	0.46
120	35	0.52
130	40	0.58

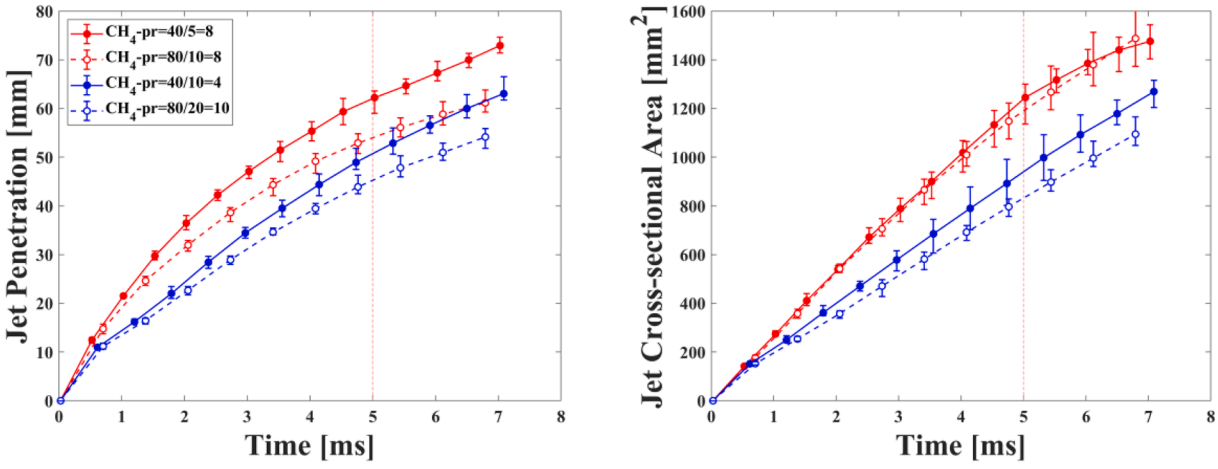

(a) Jet penetration (left) and jet cross-sectional area (right) at pr =4 and 8 for CH_4

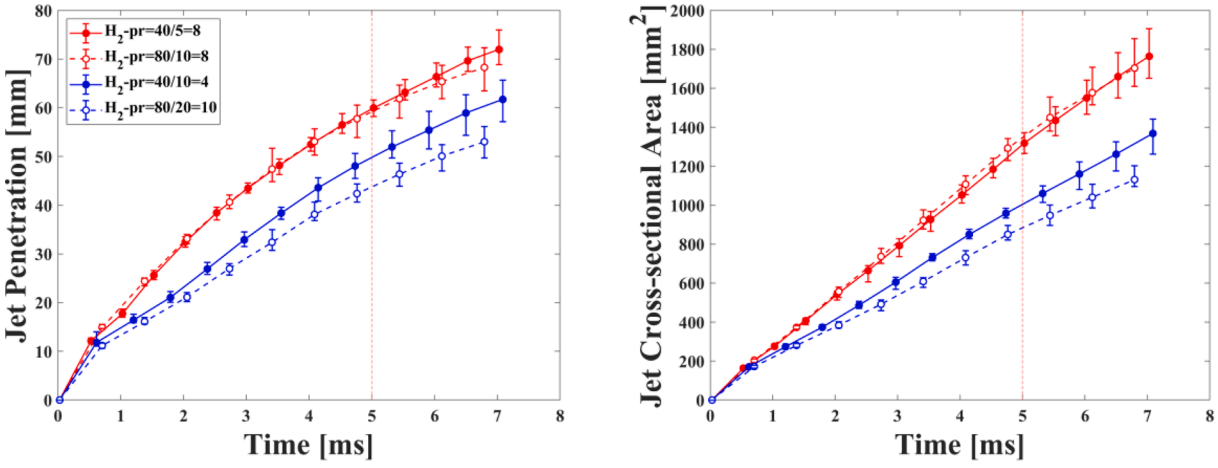

(b) Jet penetration (left) and jet cross-sectional area (right) at pr =4 and 8 for H_2

Fig. 10. Different jet characteristics at the same pressure ratio (pr).

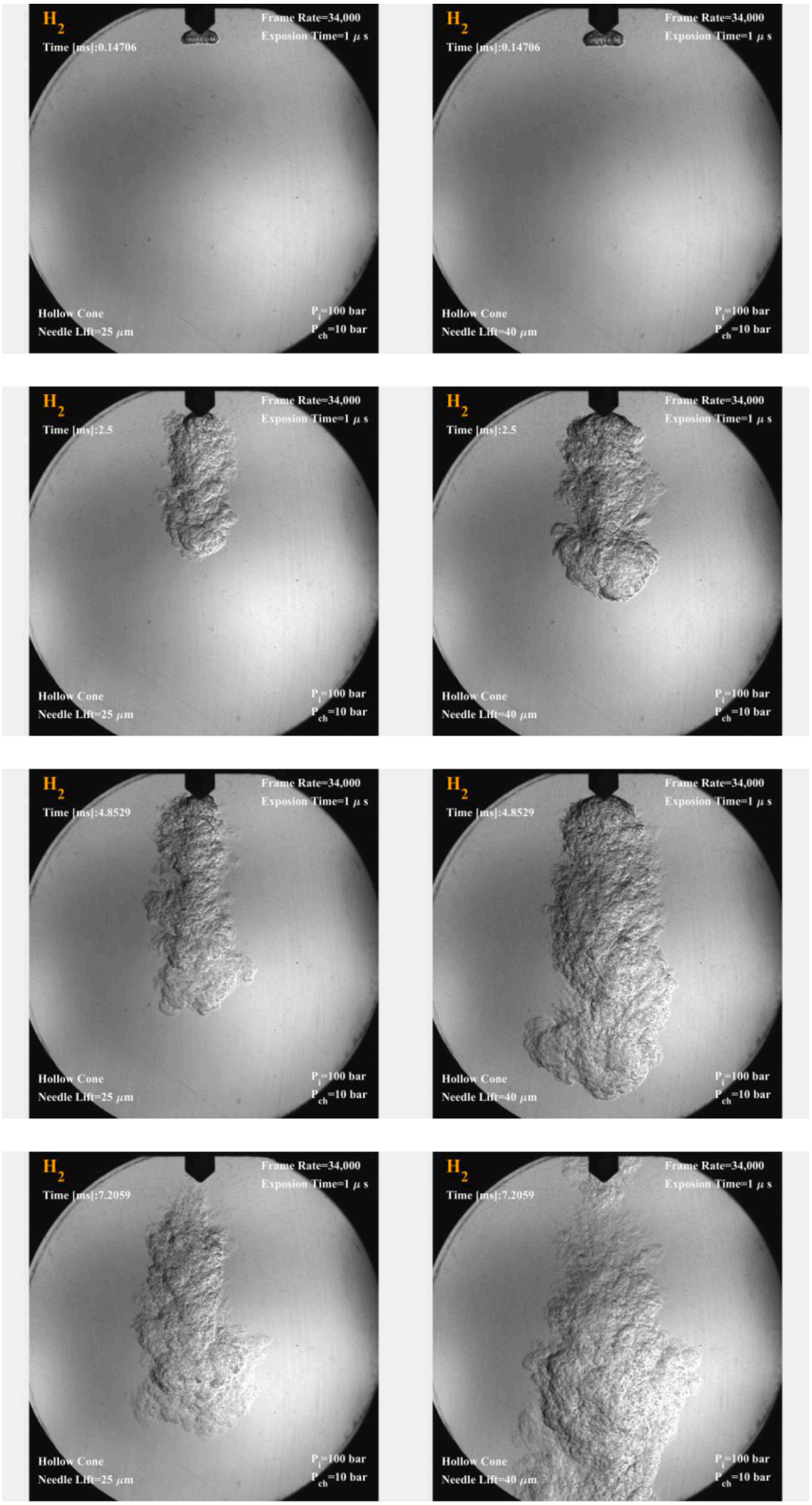

(a) H_2 jet structure at needle lift = 25μm (left) and needle lift = 40μm (right)

Fig. 11. Effect of the needle lift on the jet structure.

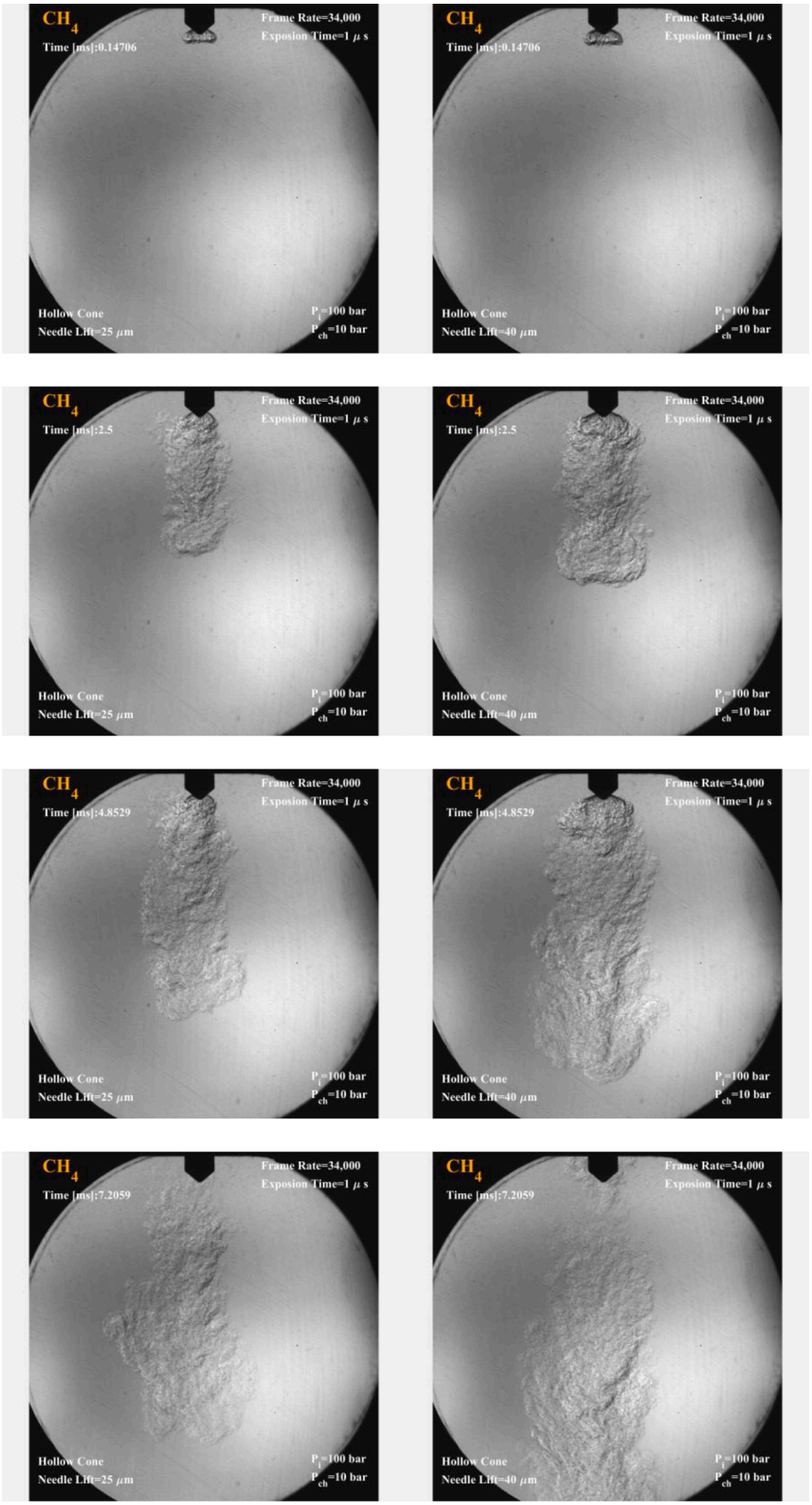

(b) CH_4 jet structure needle lift = 25μm (left) and needle lift = 40μm (right)

Fig. 11. (*continued*).

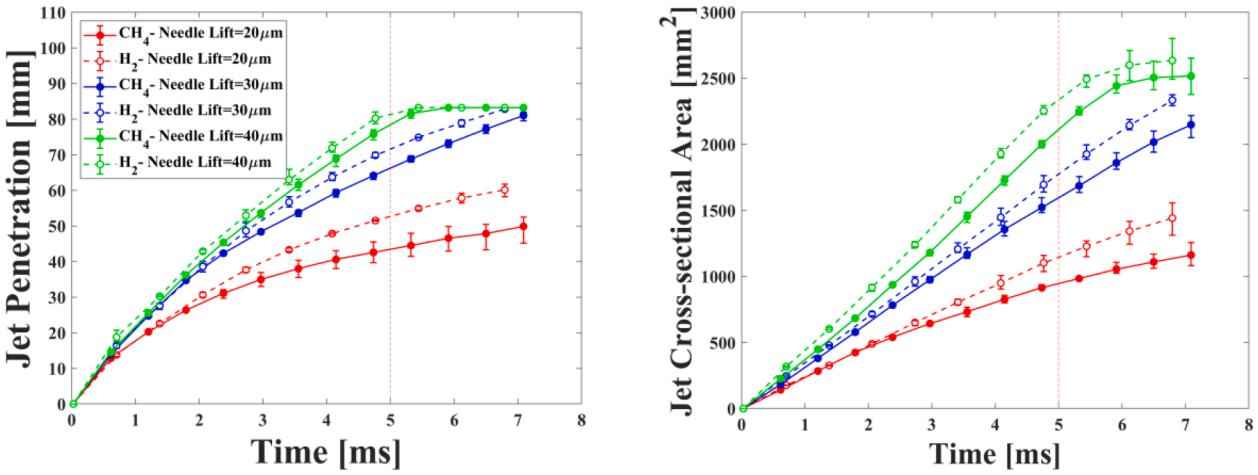

Fig. 12. Effect of the needle lift on the jet penetration and cross-sectional area at P_i = 100 bar and P_{ch} = 10 bar.

Table 6
Maximum differences between CH_4 and H_2 jet characteristics at different needle lifts.

Needle Lift (μm)	Penetration Difference (%)	Cross-sectional Area Difference (%)
20	7.5	5
30	6	5
40	2	6

3.4. Comparison of the jet characteristics from different nozzle geometries

This section presents the differences between the jet characteristics from two different nozzle geometries. For this comparison, a single-hole cap is installed on the same injector with a hollow-cone outwardly opening nozzle. However, installing the cap on the nozzle exit causes pressure loss which should be considered to reach reliable results. Two methods are applied for calculating the pressure loss in the measurements: CFD simulations (Unsteady Reynolds-Averaged Navier-Stokes (URANS) simulations of supersonic flow in the commercial software Star-CCM+ [47]) and GT-power simulations [34]. In CFD simulations, the inlet pressure is changed randomly to find the inlet pressure at which the same jet characteristics can be observed as in experiments. In GT-power simulations, it is tried to find the pressure loss based on the type of the injected gas and dimensions of the cap. The results of applying both methods show that placing the single-hole cap on the hollow-cone outwardly opening nozzle, can cause around 50% pressure loss. As an example, when the injection pressure is 100 bar for the hollow-cone outwardly opening nozzle without any caps, after placing a single-hole cap on the same nozzle, the injection pressure is 50 bar.

Fig. 13 displays the difference between a single-hole and hollow-cone jet characteristics at pr = 5, 10, and 20. As it can be seen, apart from the type of the injected gas, the single-hole and hollow-cone jet cross-sectional area do not show great differences (the maximum difference is less than 20%). However, there is a large gap between the single-hole and the hollow-cone jet penetration such that the single-hole jet penetration speed is at least 68% higher than that of the hollow-cone jet. In addition, H_2 possesses a greater jet penetration and cross-sectional area than CH_4 in all the cases which means that H_2 can provide a better mixture formation. Therefore, it can be concluded that although using the single-hole cap causes pressure loss, it can enhance the jet penetration and provide enough jet cross-sectional area for better mixture formation within a shorter time.

4. Summary and conclusions

This paper presents an experimental investigation, visualization, and comparison of the CH_4 and H_2 jets dynamics. The jets characteristics (penetration length and cross-sectional area) are studied with respect to the pressure ratio defined as the ratio of the injection pressure (P_i) to the chamber pressure (P_{ch}) (pr = 2, 3, 4, 5, 6, 8, 10, 12, 16, 20) and the needle lift (20, 25, 30, 35, and 40 μm). The characteristic differences between a hollow-cone and a single-hole jet are also investigated by placing a single-hole cap on the same injector with a hollow-cone outwardly opening nozzle. The main conclusions are as follows:

1. Despite the large differences between CH_4 and H_2 physical properties, the jet penetrations are almost similar. However, for all the cases and especially at lower injection and chamber pressures, H_2 possesses a greater jet cross-sectional area (at least 3.5% larger than CH_4) which is the main representative of efficient mixing. Thus, H_2 seems to provide a better mixture formation than CH_4.

2. Increasing the pressure ratio results in a longer jet penetration and a larger cross-sectional area. A 20% increase in the pressure ratio leads to at least 13% increase in the H_2 jet penetration and 20% increase in its cross-sectional area. The same amount of increase in the pressure ratio also increases the CH_4 jet penetration by at least17% and its cross-sectional area by at least 21%.

3. Increasing the injection pressure results in a greater jet penetration and cross-sectional area due to a higher mass flow and choked flow condition. Conversely, an increase in the chamber pressure leads to a reduced jet penetration and cross-sectional area because of the increased drag force against the jet expansion.

4. Raising the needle lift results in a larger nozzle cross-sectional area for the flow passing through and a greater mass flow rate which leads to a deeper jet penetration and a larger jet cross-section area.

5. Placing a single-hole cap on the same hollow-cone outwardly opening nozzle causes a great pressure loss (50%). However, the single-hole jet could still provide deeper penetration and enough cross-sectional area for efficient mixing.

Overall, the main outcome of this study is that although H_2 and CH_4 jet penetration are almost similar, the H_2 jet possesses a larger cross-sectional area which is representative of a better mixture formation. Apart from the type of the gas, increasing both the pressure ratio and the needle lift result in deeper jet penetration, larger cross-sectional area, and consequently higher mixing efficiency. However, it is recommended to investigate the effect of pressure ratio by changing injection pressure and chamber pressure, separately because it is shown that the jet characteristics are not the same at identical pressure ratios. Furthermore, it is

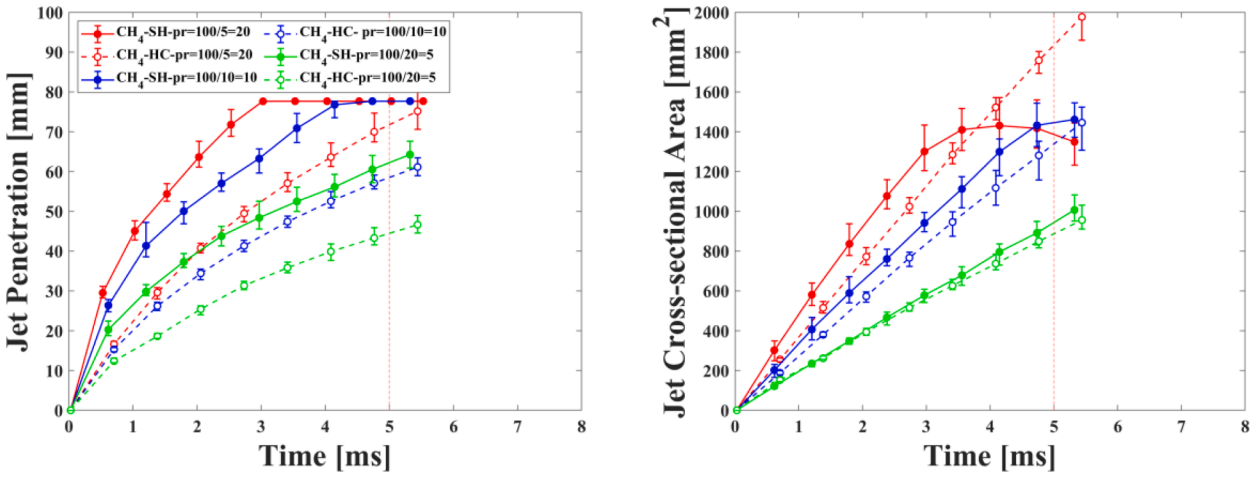

(a) CH_4 single-hole (SH) vs. hollow-cone (HC) jet penetration (left) and cross-sectional area (right)

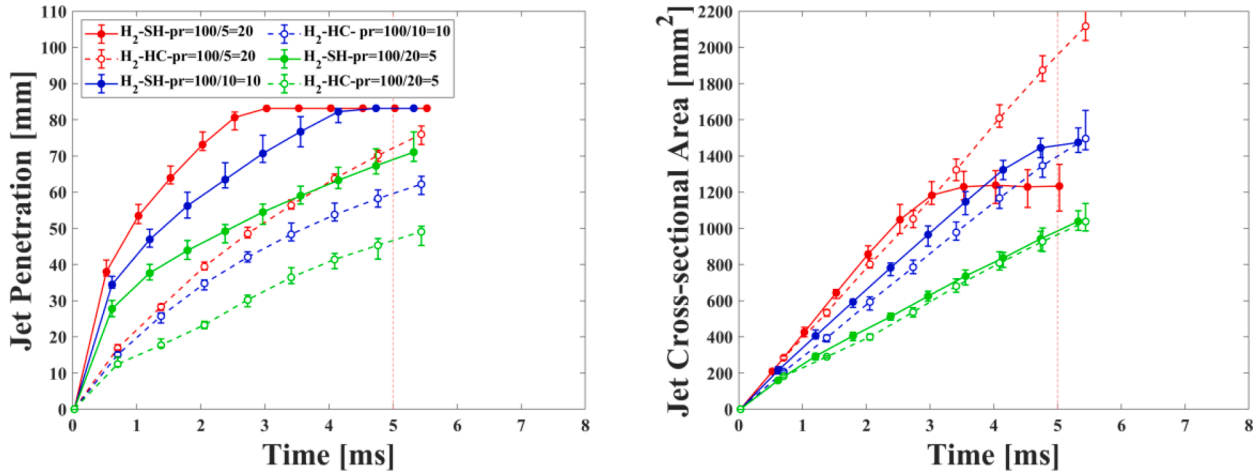

(b) H_2 single-hole (SH) vs. hollow-cone (HC) jet penetration (left) and cross-sectional area (right)

Fig. 13. CH_4 and H_2 single-hole vs hollow-cone jet characteristics at P_i = 100 bar and P_{ch} = 5, 10 and 20 bar.

shown that placing a single-hole cap on the same hollow-cone outwardly opening nozzle causes a great pressure loss but still can provide adequate mixing parameters. Further studies on the jet characteristics with a wide range of pressure ratios and different caps on the same nozzle are recommended for future work.

CRediT authorship contribution statement

Maryam Yeganeh: Investigation, Software, Formal analysis, Visualization, Funding acquisition, Writing – original draft, Writing – review & editing. **Qiang Cheng:** Conceptualization, Investigation, Software, Supervision, Writing – review & editing. **Aishwarya Dharamsi:** Investigation, Software. **Shervin Karimkashi:** Resources, Writing – review & editing. **Ossi Kaario:** Resources, Supervision, Writing – review & editing. **Martti Larmi:** Supervision, Funding acquisition, Writing – review & editing.

Declaration of Competing Interest

The authors declare that they have no known competing financial interests or personal relationships that could have appeared to influence the work reported in this paper.

Data availability

Data will be made available on request.

Acknowledgement

The authors would like to thank MSc. Olli Ranta and MSc. Otto Blomstedt for their technical assistance. The receipt of the financial support for this research work and authorship by Aalto University School of Engineering Department of Mechanical Engineering, the Academy of Finland (grant no. 141921202), and Fortum-Neste Foundation (grant no.20210162) is also acknowledged.

References

[1] bp. Statistical Review of World Energy, https://www.bp.com/en/global/corporate/energy-economics/statistical-review-of-world-energy/ ; 2021 [accessed 3 May 2022].
[2] Spencer T, Pierfederici R, Sartor O, Berghmans N, Samadi S, Fischedick M, et al. Tracking sectoral progress in the deep decarbonisation of energy systems in Europe. Energy Policy 2017;110:509–17.
[3] White CM, Steeper RR, Lutz AE. The hydrogen-fueled internal combustion engine: A technical review. Int J Hydrogen Energy 2006;31:1292–305. https://doi.org/10.1016/j.ijhydene.2005.12.001.

[4] ENERGY.GOV. Office of Energy Efficiency & Renewable Energy: Hydrogen and Fuel Cell Technologies Office, "Hydrogen production", https://www.energy.gov/eere/fuelcells/hydrogen-production; [accessed 3 May 2022].

[5] Karimkashi S, Kahila H, Kaario O, Larmi M, Vuorinen V. Numerical study on tri-fuel combustion: Ignitionproperties of hydrogen-enriched methane-dieseland methanol-diesel mixtures. Int J Hydrogen Energy 2020;45:4946–62. https://doi.org/10.1016/j.ijhydene.2019.12.033.

[6] Collodi G. Hydrogen production via steam reforming with CO2 capture. Chem Eng Trans 2010;19:3–42. https://doi.org/10.3303/CET1019007.

[7] Santhanam KSV, Press RJ, Miri MJ, Bailey AV, Takacs GA. Introduction to hydrogen technology. 2nd ed. John Wiley & Sons; 2017.

[8] Yu J, Vuorinen V, Kaario O, Sarjovaara T, Larmi M. Visualization and analysis of the characteristics of transitional underexpanded jets. Int J Heat Fluid Flow 2013;44:140–54. https://doi.org/10.1016/j.ijheatfluidflow.2013.05.015.

[9] Sankesh D, Petersen P, Lappas P. Flow characteristics of natural-gas from an outward-opening nozzle for direct injection engines. Fuel 2018;218:188–202. https://doi.org/10.1016/j.fuel.2018.01.009.

[10] Wang X, Sun B, Luo Q, Bao L, Su J, Liu J, et al. Visualization research on hydrogen jet characteristics of an outward opening injector for direct injection hydrogen engines. Fuel 2020;280:118710. https://doi.org/10.1016/j.fuel.2020.118710.

[11] Duan J, Liu F, Sun B. Backfire control and power enhancement of a hydrogen internal combustion engine. Int J Hydrogen Energy 2014;39(9):4581–9. https://doi.org/10.1016/j.ijhydene.2013.12.175.

[12] Luo QH, Sun BG. Inducing factors and frequency of combustion knock in hydrogen internal combustion engines. Int J Hydrogen Energy 2016;41(36):16296–305.

[13] Kalam M, Masjuki H. An experimental investigation of high performance natural gas engine with direct injection. Energy 2011;36(5):3563–71. https://doi.org/10.1016/j.energy.2011.03.066.

[14] Li T, Moriwaki R, Ogawa H, Kakizaki R, Murase M. Dependence of premixed low-temperature diesel combustion on fuel ignitability and volatility. Int J Engine Res 2011;13(1):14–27. https://doi.org/10.1177/1468087411422852.

[15] Yu J, Vuorinen V, Kaario O, Sarjovaara T, Larmi M, Sarjovaara. , Characteristics of high pressure jets for direct injection gas engine. SAE Internat J Fuels Lubric 2013;6(1):149–56.

[16] Kuensch Z, Schlatter S, Keskinen K, Hulkkonen T, Larmi M, Boulouchos K. Experimental investigation on the gas jet behavior for a hollow cone piezoelectric injector. SAE Technical Paper 2014;01:2749. https://doi.org/10.4271/2014-01-2749.

[17] Abraham J, Magi V, MacInnes J, Bracco F. Gas versus spray injection: which mixes faster?. In: SAE Technical Paper 940895; 1994. https://doi.org/10.4271/940895.

[18] Yu J, Hillamo H, Sarjovaara T, Hulkkonen T, Kaario T, Larmi M. Experimental study on structure and mixing of low-pressure gas jet using tracer-based PLIF technique. SAE Technical Paper 2011;24:0039. https://doi.org/10.4271/2011-24-0039.

[19] Yu J, VuorinenV Hillamo H, Sarjovaara T, Kaario O, Larmi M. An experimental study on high pressure pulsed jets for DI gas engine using planar laser-induced fluorescence. In: SAE Technical Paper 2012; 2012. p. 1655. https://doi.org/10.4271/2012-01-1655.

[20] Vuorinen V, Yu J, Tirunagari S, Kaario O, Larmi M, Duwig C, et al. Large-eddy simulation of highly underexpanded transient gas jets. Phys Fluids 2013;25(1):016101.

[21] Yu J, Vuorinen V, Hillamo H, Sarjovaara T, Kaario O, Larmi M. An experimental investigation on the flow structure and mixture formation of low-pressure ratio wall-impinging jets by a natural gas injector. J Nat Gas Sci Eng 2012;9:1–10. https://doi.org/10.1016/j.jngse.2012.05.003.

[22] Yu J, Hillamo H, Vuorinen V, Sarjovaara T, Kaario O, Larmi M. Experimental investigation of characteristics of transient low-pressure wall-impinging gas jet. J Phys Conf Ser 2011;318(032047). https://iopscience.iop.org/article/10.1088/1742-6596/318/3/032047/pdf. https://doi.org/10.1088/1742-6596/318/3/032047.

[23] Vera-Tudela W, Kyrtatos P, Schneider B, Boulouchos K, Willmann M. An experimental study on the effects of needle dynamics on the penetration of a high-pressure methane jet. Fuel 2019;253:79–89. https://doi.org/10.1016/j.fuel.2019.04.171.

[24] Thurnheer T, Soltic P, Dimopoulos EP. S.I.engine fuelled with gasoline, methane and methane/hydrogen blends: heat release and loss analysis. Int J Hydrogen Energy 2009;34:2494–503. https://doi.org/10.1016/j.ijhydene.2008.12.048.

[25] Mohammed MK, Rahman M, Abu Bakar R, Kadirgama K. Modeling of SI engine for duel fuels of hydrogen, gasoline and methane with port injection feeding system. Energy Educ Sci Technol 2012;29:1399–416.

[26] Das L, Gulati R, Gupta P. A comparative evaluation of the performance characteristics of a spark ignition engine using hydrogen and compressed natural gas as alternative fuels. Internat J Hydrogen Energy 2000;25:783e93. https://doi.org/10.1016/S0360-3199(99)00103-2.

[27] Akansu S, Dulger Z, Kahraman N, Veziroglu T. Internal combustion engines fueled by natural gasdhydrogen mixtures. Internat J Hydrogen Energy 2004;29:1527e39. https://doi.org/10.1016/J.IJHYDENE.2004.01.018.

[28] Karim G, Wierzba I, Al-Alousi Y. Methane-hydrogen mixtures as fuels. Internat J Hydrogen Energy 1996;21:625e31. https://doi.org/10.1016/0360-3199(95)00134-4.

[29] iea Hydrogen. Global Outlook and Trends for Hydrogen, http://ieahydrogen.org/pdfs/Global-Outlook-and-Trends-for-Hydrogen/; 2017 [accessed 15 July 2021].

[30] Abdul Rahman MT, Kawahara N, Tsuboi K, Tomita E. Effect of ambient pressure on local concentration measurement of transient hydrogen jet in a constant-volume vessel using spark-induced breakdown spectroscopy. Int J Hydrogen Energy 2015;40(13):4717–25.

[31] Deng J, Zhong H, Gong Y, Gong X, Li L. Studies on injection and mixing characteristics of high-pressure hydrogen and oxygen jet in argon atmosphere. Fuel 2018;226:454–61.

[32] Takagi Y, Oikawa M, Sato R, Kojiya Y, Mihara Y. Near-zero emissions with high thermal efficiency realized by optimizing jet plume location relative to combustion chamber wall, jet geometry and injection timing in a direct-injection hydrogen engine. Int J Hydrogen Energy 2019;44:9456–65. https://doi.org/10.1016/j.ijhydene.2019.02.058.

[33] Wang J, Huang Z, Miao H, et al. Characteristics of direct injection combustion fueled by natural gas-hydrogen mixtures using a constant volume vessel. Int J Hydrogen Energy 2008;33:1947–56. https://doi.org/10.1016/j.ijhydene.2008.01.007.

[34] GAMMA TECHNOLOGIES. WHAT IS GT-POWER?, https://www.gtisoft.com/gt-power/ 2022; [accessed 3 May 2022].

[35] ni. What Is LabVIEW?, https://www.ni.com/fi-fi/shop/labview.html#; 2022 [accessed 3 May 2022].

[36] Settles GS. Schlieren and shadowgraph techniques visualizing phenomena in transparent media. 1st ed. Berlin, Heidelberg: Springer; 2009. https://doi.org/10.1007/978-3-642-56640-0.

[37] Petrucci RH, Harwood WS, Herring FG. General chemistry. 8th ed. Upper Saddle River, N.J.: Prentice HallPrentice-Hall; 2002.

[38] Donaldson C, Snedeker R. A study of free jet impingement. Part 1. Mean properties of free and impinging jets. J Fluid Mech 1971;45(2):281–319. https://doi.org/10.1017/S0022112071000053.

[39] Perry RH, Green DW. Perry's chemical engineers' handbook. 8th ed. New York: McGraw-Hill; 2007.

[40] Sakellarakis V, Vera-Tudela W, Doll U, Ebi D, Wright Y, Boulouchos K. The effect of high-pressure injection variations on the mixing state of underexpanded methane jets. Int J Engine Res 2021;22(9):2900–18. https://doi.org/10.1177/1468087420960895.

[41] Banholzer M, Vera-Tudela W, Traxinger C, Pfitzner M, Wright Y, Boulouchos K. Numerical investigation of the flow characteristics of underexpanded methane jets. Phys Fluids 2019;31(5):056105.

[42] Nouri J, Whitelaw JH. Effect of chamber pressure on the spray structure from a swirl pressure atomiser for direct injection gasoline engines. Inst Phys Conf Ser 2003;177:121–30. https://doi.org/10.1201/b16835-23.

[43] Hollingshead CL, Johnson MC, Barfuss SL, Spall RE. Discharge coefficient performance of Venturi, standard concentric orifice plate, V-cone and wedge flow meters at low Reynolds numbers. Petrol Sci Eng 2011;78(3–4):559–66. https://doi.org/10.1016/j.petrol.2011.08.008.

[44] Science Direct. Discharge Coefficient, https://www.sciencedirect.com/topics/engineering/discharge-coefficient.

[45] The Engineering ToolBox. Gases - Dynamic Viscosities, https://www.engineeringtoolbox.com/gases-absolute-dynamic-viscosity-d_1888.html.

[46] CHEMISTRY. Chapter 7.2: Intermolecular forces, https://chem.libretexts.org/Courses/Prince_Georges_Community_College/CHEM_2000%3A_Chemistry_for_Engineers_(Sinex)/Unit_3%3A_States_of_Matter/Chapter_7%3A_Fluids/Chapter_11.02%3A_Intermolecular_forces. [accessed 3 May 2022].

[47] SIEMENCE. Simcenter STAR-CCM+, https://www.plm.automation.siemens.com/global/en/products/simcenter/STAR CCM.html. 2022 [accessed 3 May 2022].